JOURNAL OF MATERIALS SCIENCE 24 (1989) 154–162

Effect of dynamic recrystallization on the importance of grain-boundary sliding during creep

M. R. DRURY*
Institute of Earth Sciences, State University of Utrecht, Budapestlaan 4, 3584 CD Utrecht, Netherlands

F. J. HUMPHREYS, S. H. WHITE‡
Department of Metallurgy and Materials Science, and ‡Department of Geology, Imperial College, London SW7 2BP, UK

During creep of polycrystalline materials at elevated temperatures, a certain amount of the strain is accommodated by grain-boundary sliding (GBS). The relative importance of GBS depends on the stress and grain size and sometimes temperature. During high-strain deformation, dynamic recrystallization often occurs with the resultant grain size only related to the stress. In this situation the importance of GBS is then dependent only upon stress and sometimes temperature. In dynamically recrystallized Magnox Al80 deformed at $T > 0.8\,T_m$, 16 to 23% of the imposed strain is accommodated by GBS. A comparison has been made between the experimental results and some theoretical models for the importance of GBS during creep, modified to take account of recrystallization. The best fit to the data is obtained with the modified form of Langdons model. Deformation mechanism maps constructed with this model suggest that dynamic recrystallization can cause a switch of mechanism from dislocation creep to dominant GBS at intermediate temperature ($T < 673$ K) and low stress. Deformation mechanism maps have also been constructed for calcite based on the data of Schmid *et al.* These suggest that GBS is an important mechanism in calcite deformed under geological conditions.

1. Introduction

During creep of polycrystalline materials at elevated temperatures ($T > 0.5\,T_m$) strain is accommodated by intragranular and grain-boundary deformation mechanisms. The relative importance of the types of mechanism determine if there is any grain size sensitivity of the creep strength.

It is well established that during dislocation creep at low normalized stress, a certain amount of strain is accommodated by grain-boundary sliding [1–8]. The relative importance of grain-boundary sliding (GBS) is usually expressed as

$$E = \varepsilon_s/\varepsilon_t \quad (1)$$

where ε_s is the strain due to GBS and ε_t the total strain.

Low-strain creep experiments have established that E increases with decreasing stress [1, 4, 7] and decreasing grain size [1, 4, 9] while the temperature dependence varies. In aluminium, E is temperature independent from 533 to 748 K [2, 9] while in Magnox Al80 (Mg0.8%Al), E is temperature independent at $T < 473$ K and decreases with increasing temperature in the range 473 to 573 K [4].

During high-strain dislocation creep many materials recrystallize [10–14] and studies on a wide range of metals, ceramics and minerals [11, 13, 15, 16] indicate that the dynamically recrystallized grain size (d) is only related to the steady state stress

$$d = B\sigma^{-z} \quad (2)$$

where B and z are both constants.

As dynamic recrystallization alters the grain size its occurrence will effect the importance of GBS. It is possible that a drastic grain-size reduction due to recrystallization can cause a change of the dominant deformation mechanism from dislocation creep to GBS [17, 18]. This is potentially an important way of producing localized shear bands and shear zones by inhomogeneous recrystallization [19, 20].

In this contribution, the effect of dynamic recrystallization on the importance of GBS has been studied in Mg0.8%Al, 0.005% Be – a single-phase magnesium alloy known as Magnox Al80. The results have been compared with some theoretical models regarding the importance of GBS, which have been modified to take account of dynamic recrystallization. The develop-

Present address: Mineralogy Research Centre, Research School of Chemistry, Australian National University, Canberra A.C.T. 2601, Australia.

0022–2461/89 $03.00 + .12

ment of microstructure and the recrystallization mechanisms in Magnox Al80 have been described elsewhere [15, 21]. Comparison is also made between the theoretical models and available data for calcite ($CaCO_3$) [8, 22] which is an important rock-forming mineral.

2. Experimental methods

2.1. Deformation tests

Magnox Al80 was obtained from Magnesium Electron Ltd. Cylindrical specimens were machined from extruded rods and chemically polished to remove any surface deformation. Deformation tests were performed at constant displacement rate in an Instron testing machine in the temperature range $T = 873$ to 573 K and strain rates $\dot{\varepsilon} = 5 \times 10^{-6}$ sec^{-1} to 2×10^{-3} sec^{-1}.

Measurements of the amount of strain accommodated by GBS were made on three split cylinder specimens [23] deformed at 748, 823 and 873 K at $\dot{\varepsilon} = 2 \times 10^{-4}$ sec^{-1}. These specimens were deformed to $\varepsilon = 0.42$, water quenched and longitudinally sectioned by spark erosion. The internal surfaces were polished and etched and finally a grid of 25 μm diameter gold squares was evaporated on to one of the surfaces. The specimens were subsequently reassembled and deformed a second time by a small increment of $\varepsilon = 0.05$ to 0.01. Tests on a specimen in which a thermocouple had been embedded showed that a heating of 2 to 5 min was sufficient to achieve the stable deformation temperature. The shortest possible time was used to reduce the effects of static recovery.

2.2. Measurement of strain due to GBS (ε_s)

The magnitude of ε_s accommodated during the second deformation stage has been calculated from displacements of the grid lines [24]

$$\varepsilon_s = k\bar{\omega}/L \qquad (3)$$

where $\bar{\omega}$ is the mean grain-boundary displacement of a grid line in a direction perpendicular to the compression axis (Fig. 1) [25], L is the mean linear intercept of the grains parallel to the compression axis and k is a geometric averaging factor [26] which is constant for a particular type of microstructure.

In all, 180 to 190 individual displacements were measured on each specimen. Measurements were made using the eyepiece graticule of a light microscope. Each displacement was assigned to graticule intervals of 2.4 μm width and the mean value was calculated using the approximation $\bar{\omega} = \Sigma f\omega_n/\Sigma f$ where ω_n represents the mid-values of the graticule intervals, e.g. $\omega_1 = 1.2\,\mu$m, $\omega_2 = 3.6\,\mu$m, $\omega_3 = 6\,\mu$m. The value of $\bar{\omega}$ obtained in this way is probably a slight overestimate [27].

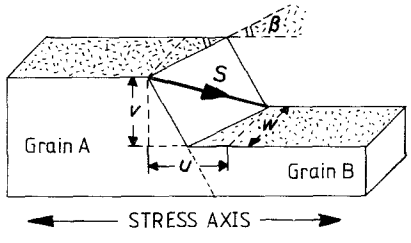

Figure 1 Measurement of grain-boundary sliding displacements. The true sliding vector, S, can be divided into three perpendicular components, u parallel to the stress axis, v parallel to the normal of the observation surface, and w perpendicular to the stress axis, in the surface observation plane.

The value of the geometric averaging factor, k, is dependent upon the grain-boundary configuration. A theoretical method described by Bell *et al.* [25] has been used to estimate k for the high-strain dynamic recrystallized microstructures.

From Equation 3

$$K = 2\sum_{0}^{90}\left[\frac{\omega(\beta)f(\beta)}{\tan\beta}\right]\Big/\sum_{0}^{90}[\omega(\beta)f(\beta)] \qquad (4)$$

where $f(\beta)$ is the frequency of occurrence of boundaries with angle β to the compression axis, and $\omega(\beta)$ may be approximated by the average displacement for boundaries of angle β [28]. The two summations in Equation 4 were evaluated using a theoretical distribution curve for $\bar{\omega}(\beta)$ [28] and an experimentally determined distribution curve for $f(\beta)$ [27]. The value of $k = 1.26$ was obtained, which compares with a value of $k = 1.44$ to 1.66 found by Bell *et al.* [25] for an equiaxed polygonal microstructure.

In high-strain compression tests, bulk deformation is quite inhomogeneous because of frictional effects at the ends of the specimen. The sliding displacement measurements (ω) were taken from the central zone of the specimen, where the total strain is higher than in the bulk. The magnitude of ε_t used to calculate $E = \varepsilon_s/\varepsilon_t$, was directly obtained from measurements of the total strain of the 25 μm grid, in the central part of the specimen.

3. Results

3.1. Mechanical behaviour

True stress, true strain curves are shown in Fig. 2. At high stress ($\sigma \sim 15$ to 25 MPa) the curves have a sharp peak at $\varepsilon \sim 0.1$, thereafter the stress decreases until $\varepsilon \sim 0.4$ to 0.6 where it attains a steady value. At

TABLE I Mechanical data for Magnox Al80 at $T > 570$ K

T (K)	$\dot{\varepsilon}$ (sec^{-1})	Peak stress (MPa)	Final stress (MPa)
673	2×10^{-3}	21.0	15.8
703	2×10^{-3}	17.5	12.7
733	2×10^{-3}	12.5	10.0
773	2×10^{-3}	7.3	6.9
798	2×10^{-3}	6.7	6.4
823	2×10^{-3}	–	5.0
848	2×10^{-3}	–	4.3
873	2×10^{-3}	–	3.4
673	2×10^{-4}	16.0	12.3
698	2×10^{-4}	13.3	10.7
723	2×10^{-4}	9.6	8.3
748	2×10^{-4}	8.0	6.8
773	2×10^{-4}	6.0	5.7
823	2×10^{-4}	–	3.2
873	2×10^{-4}	–	2.3
573	5×10^{-6}	20.1	13.1
673	5×10^{-6}	10.4	7.7
723	5×10^{-6}	–	3.2
773	5×10^{-6}	–	2.0
823	5×10^{-6}	–	1.4
823	5×10^{-3}	–	7.3
823	5×10^{-5}	–	2.6

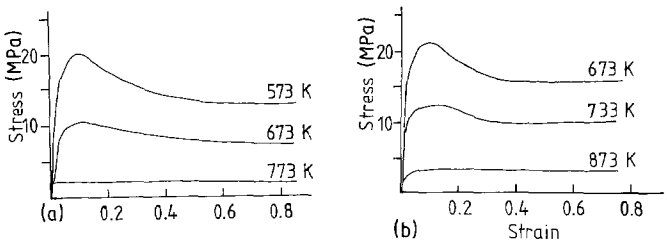

Figure 2 True stress, true strain curves for Magnox Al80 deformed at $T > 570$ K. (a) $\dot{\varepsilon} = 5 \times 10^{-6}$ sec^{-1}, (b) $\dot{\varepsilon} = 2 \times 10^{-3}$ sec^{-1}.

low stress ($\sigma < 5$ MPa) a steady stress is attained after small strains, $\varepsilon \sim 0.01$ to 0.05.

The mechanical results (Table I) can be described by a flow law of the form

$$\dot{\varepsilon} = A\sigma^p \exp(-Q/RT) \quad (5)$$

(Fig. 3a) with $p = 4$ at $T > 733$ K and $p \sim 9$ at $T < 733$ K. The apparent activation energy varies with stress (Fig. 3b) and ranges from 150 kJ mol^{-1} at 7 MPa to 240 kJ mol^{-1} at 2 MPa (Fig. 3b).

3.2. Microstructural development

The high-strain microstructures are similar over the range of conditions investigated. Initial grain sizes and shapes were completely transformed (Fig. 4) by dynamic recrystallization which occurs by a combination of grain-boundary migration and new grain-boundary formation [15]. The resultant grain size is related only to the steady state stress [15].

3.3. Split cylinder tests

The surfaces of the split cylinder tests were examined by reflected light microscopy. Limited depth of focus caused some problems, but more deformation features were visible than in scanning electron microscopy. Deformation of the grid showed that both intragranular and grain-boundary deformation mechanisms had been operative. Inside the grains, numerous parallel basal slip lines develop (Fig. 5a). Some show discrete displacements of the grid lines. The basal slip line spacing increases with increasing temperature, and at 873 K additional sets of slip lines occur (Fig. 5b) which have a closer spacing than the basal slip lines and a characteristic segmented geometry.

A variety of deformation markings were observed at grain boundaries (Fig. 5c, d) depending on the relative importance of grain-boundary sliding and migration. Boundaries which did not migrate show a single sliding displacement discontinuity, while migrated boundaries show a number of discontinuities associated with intermediate positions of the boundary. Rotation of the grid line between the sliding discontinuities indicates that sliding was continuous with spasmodic grain-boundary migration [29]. The close association of sliding and migration shows that the migration occurred during deformation and not in the heating up period prior to the second deformation.

Values of the mean GBS displacement, $\bar{\omega}$, and the derived values of ε_s, ε_t and E are shown in Table II. Grain-boundary sliding accommodates 16 to 23% of the imposed deformation with E increasing as the temperature decreases and stress increases.

4. Discussion

4.1. Theoretical models for E

A number of theoretical models for E as a function of stress, grain size and temperature have been developed [6, 7, 30]. Those due to Gifkins [6] and Langdon [7] can be simply modified to take account of dynamic recrystallization.

In Langdons model it is assumed that GBS is an independent mechanism such that E can be expressed in terms of strain rates.

$$E = \dot{\varepsilon}_s/\dot{\varepsilon}_s + \dot{\varepsilon}_g \quad (6)$$

where $\dot{\varepsilon}_g$ is the strain rate due to intragranular deformation mechanisms. Substituting the flow laws for dislocation creep (Equation 7) and for GBS (Equation 8)

$$\dot{\varepsilon}_g = K\sigma^p \exp(-Q_g/RT) \quad (7)$$

$$\dot{\varepsilon}_s = J\sigma^q d^{-m} \exp(-Q_s/RT) \quad (8)$$

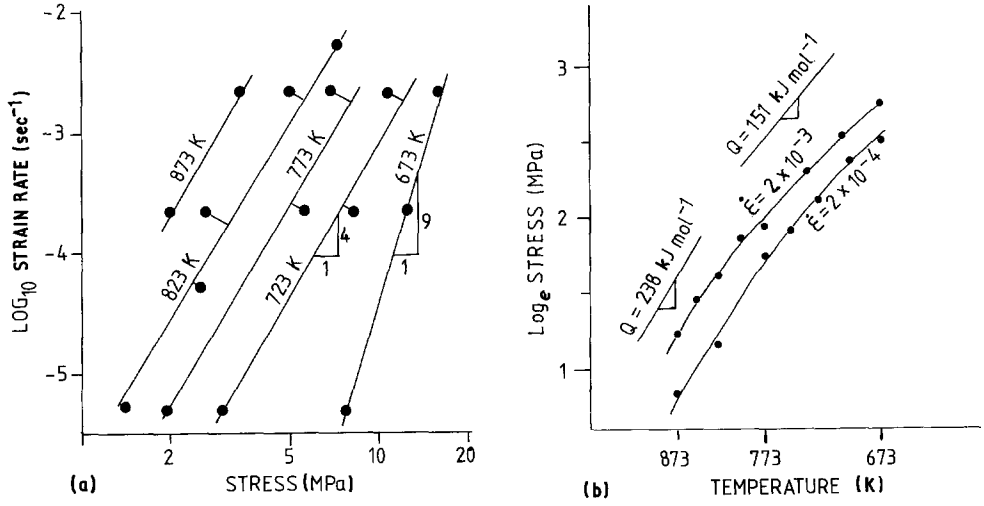

Figure 3 Dependence of flow stress upon (a) strain rate and (b) temperature for Magnox Al80 deformed at $T > 570$ K.

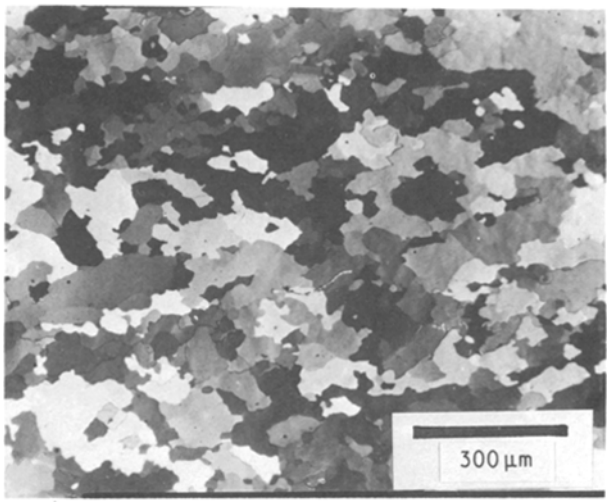

Figure 4 High strain completely recrystallized microstructure (initial grain size 1 to 3 mm) in specimen deformed at $T = 823$ K, $\dot{\varepsilon} = 2 \times 10^{-3}$ sec^{-1}.

$$E = [1 + M\sigma^{p-q}d^{m} \exp(-\Delta Q/RT)]^{-1} \quad (9)$$

(where K and J are constants and Q_g and Q_s are apparent activation energies) where $M = K/J$ and $\Delta Q = (Q_g - Q_s)$.

At high strains the initial grain size is no longer preserved. Substituting the stress/dynamic recrystallized grain size relationship (Equation 2) into Equation 9 gives

$$E = [1 + C\sigma^{p-(q+zm)} \exp(-\Delta Q/RT)]^{-1} \quad (10)$$

where $C = M/B^{-m}$. This expression predicts that the amount of strain accommodated by GBS in a dynamically recrystallized microstructure is a function of stress and possibly temperature depending on the difference (if any) between the activation energies for GBS and dislocation creep.

TABLE II Measurement of strain accommodated by GBS

T (K)	L (μm)	ω (μm)	ε_s	ε_t	E
873	360	4.5	0.015	0.095	0.16
823	307	2.8	0.010	0.05	0.20
748	173	3.1	0.021	0.09	0.23

In Gifkins [6] model, GBS is accommodated by intragranular deformation in triple-point folds. The strain rate due to sliding is controlled by the strain rate in the folds, $\dot{\varepsilon}_f$, such that

$$\dot{\varepsilon}_t = \dot{\varepsilon}_g + \dot{\varepsilon}_s + 2\dot{\varepsilon}_f \quad (11)$$

Substituting rate equations for $\dot{\varepsilon}_g$, $\dot{\varepsilon}_s$ and $\dot{\varepsilon}_f$ [6] into Equation 11 gives

$$E = 2Fay/(3d^2 + 6ay) \quad (12)$$

where F is a stress concentration factor, a is the subgrain size and y is the width of the triple-point fold. Equation 12 can be modified to take account of dynamic recrystallization and of the stress dependence of the subgrain size [13] (where $a = \alpha\sigma^{-b}$). This gives

$$E = \left[3 + \frac{3B^2\alpha}{2Fy}\sigma^{(b-2z)}\right]^{-1} \quad (13)$$

For the special case of rotation recrystallization where $d = a$, Equation 13 becomes

$$E = \left(3 + \frac{3B^3}{2Fy}\sigma^{-z}\right)^{-1} \quad (14)$$

Gifkin's [6] model with $d = a$ is equivalent to

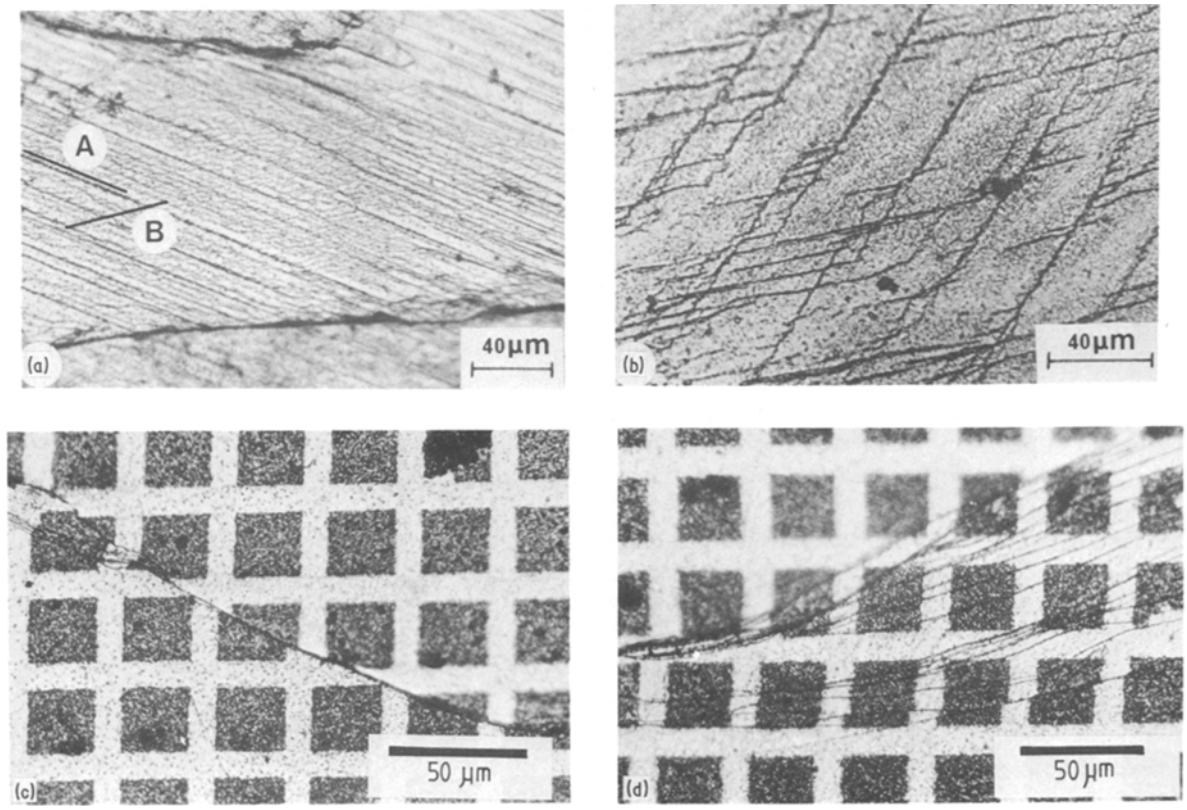

Figure 5 Deformation markings on surface of split cylinder tests. (a) Basal (A) and non-basal (B) slip lines. (b) Segmented nature of non-basal slip lines. (c) Single sliding discontinuity at immobile grain boundary. (d) Multiple sliding discontinuities produced by continuous sliding with spasmodic migration.

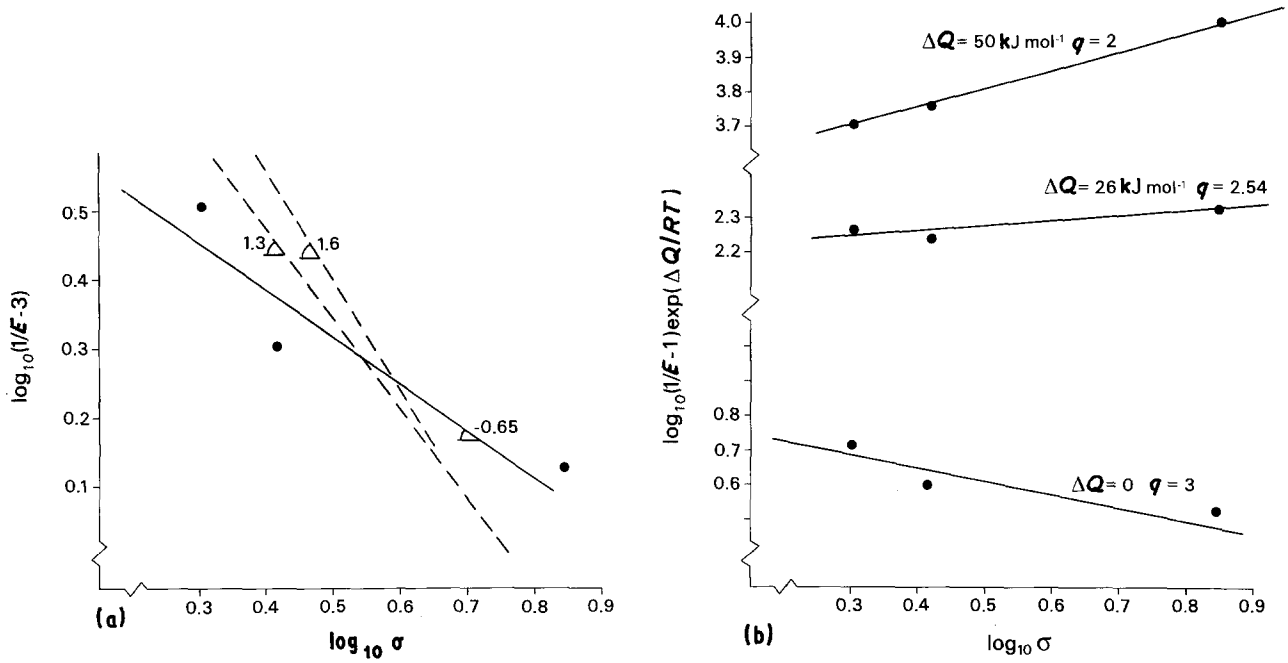

Figure 6 Comparison between theory and experimental results. (a) A plot of $\log_{10}(1/E - 3)$ against $\log_{10}\sigma$. Gifkin's theory [6] predicts a straight line of slope -1.3 to -1.6 which compares with the best fit experimental value of -0.65. (b) Plots of $\log_{10}(1/E - 1)\exp(\Delta Q/RT)$ against $\log_{10}\sigma$. A good fit to the experimental results can be obtained with Langdon's [7] theory for a range of values of ΔQ and q. Three cases are shown, $\Delta Q = 0$ and $q = 3$, $\Delta Q = 26\,\text{kJ mol}^{-1}$ and $q = 2.54$ and $\Delta Q = 50\,\text{kJ mol}^{-1}$ and $q = 2$.

Langdon's model for the case of $p = q$, $\Delta Q = 0$ and $m = 1$, while for the case of $d \neq a$ an additional stress dependence of E on the size of the triple-point fold occurs.

4.2. Comparison between theory and experiments

Gifkin's [6] model (Equations 13 and 14) predicts an effective stress dependence for E of -1.3 to -1.6. The experimentally obtained effective stress dependence is -0.65, while considerable scatter of the data points from the ideal straight line (Fig. 6a) occurs.

Comparison with Langdon's [7] model (Equation 10) has been made taking values of $p = 4$, $z = 1.3$ and $Q_g = 250$ to $150\,\text{kJ mol}^{-1}$. Values of $q = 2 - 3$, $m = 1$ and $\Delta Q = 0$ to $26\,\text{kJ mol}^{-1}$ have been extrapolated from the study of Bell and Langdon [4] who established these parameters in Magnox Al80 during creep at 398 to 573 K and $\sigma = 14$ to 55 MPa.

A fit to the experimental results can be obtained (Fig. 6b) for a number of combinations of ΔQ and q ranging from $q = 3$ and $\Delta Q = 0$ to $q = 2$ and $\Delta Q = 50\,\text{kJ mol}^{-1}$. Thus the experimental results are consistent with Langdon's model provided that GBS is controlled by a similar mechanism as the intergranular creep mechanism, i.e. either $Q_s = Q_g$ or Q_s varies with the same dependence on stress as Q_g such that ΔQ remains constant. This requires that GBS be controlled by cross slip of non-basal lattice dislocations [31].

The extrapolation of Bell and Langdon's [4] data to the conditions of this study needs some discussion and justification. The mechanical data in their study indicated the occurrence of two creep regimes. At higher stress and temperature there was evidence for non-basal slip with $p = 7$ and $Q = 210\,\text{kJ mol}^{-1}$, while at lower stress and temperature $p = 5$ and $Q = 135\,\text{kJ mol}^{-1}$. The higher stress regime has similar characteristics (i.e. high activation energy, and activation of non-basal systems) to the creep regime found in this study and that of Varigali and Langdon [31]. This provides justification for the extrapolation of the values of m, q and ΔQ to the conditions of this study. It should be noted; however, that other studies [31, 32] are not consistent with the results of Bell and Langdon [4]. These studies find a creep regime at higher temperature and stress with $p = 6$ and $Q = 135$ to $140\,\text{kJ mol}^{-1}$ and activation of non-basal slip systems was only reported at higher temperatures ($T > 673$ K) [31].

4.3. Deformation mechanism maps $E = f(\sigma, d, T)$

Deformation mechanism maps showing the importance of GBS as a function of stress, temperature and grain size can be constructed by combining the experimental results with the theoretical models. A map constructed using Langdon's [7] model is shown in Fig. 7, with the stress–dynamic recrystallized grain size relationship plotted to illustrate the effect of recrystallization. Contours of constant E are straight lines on the map with slope $-(p - q)/m$. The $E = 0.5$ contours are plotted for two cases in Fig. 7: (i) $q = 3$ and $\Delta Q = 0$, and (ii) $q = 2$, $\Delta Q = 50\,\text{kJ mol}^{-1}$. For the temperature-independent case (with dynamic recrystallization), E remains almost constant at about 0.2 with decreasing stress. For the strongest temperature dependence of $\Delta Q = 50\,\text{kJ mol}^{-1}$ at 748 K, GBS is predicted to become the dominant mechanism at stresses less than 0.9 MPa.

Another map for Magnox Al80, which includes results from low-temperature creep studies [4] is shown in Fig. 8. Contours for $E = 0.5$ are shown for 748, 573 and 473 K, clearly showing that E is temperature dependent. Langdon's model [7] provides a reasonable fit to the data over the whole temperature

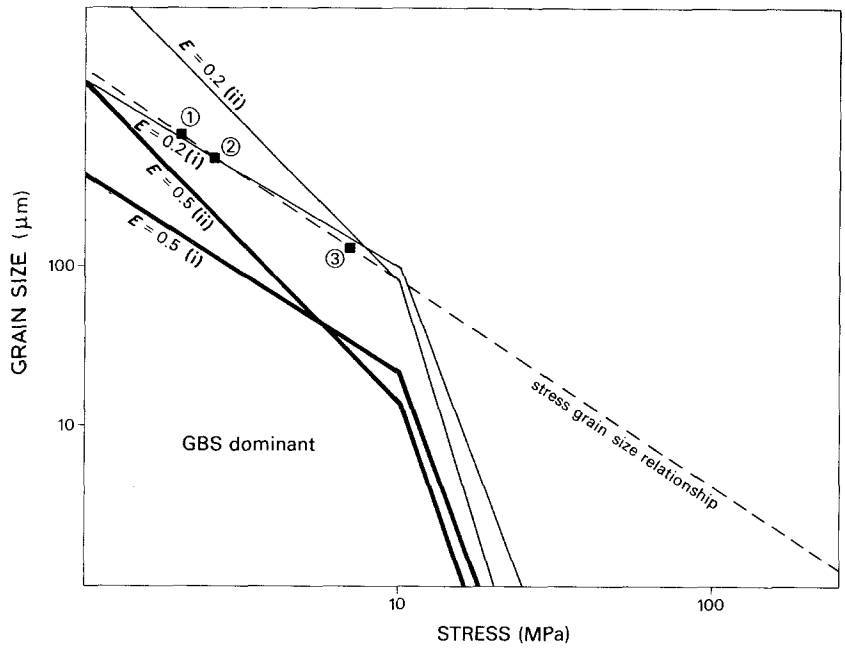

Figure 7 Deformation mechanism map for Magnox Al80 deformed at $T > 740$ K. The $E = 0.2$ and $E = 0.5$ contours have been constructed for two cases, (i) $\Delta Q = 0$ and $q = 3$, and (ii) $\Delta Q = 50\,\text{kJ mol}^{-1}$, $q = 2$ at 748 K. The slopes of the contours were obtained from Langdon's [7] model, while the positions are constrained by the experimental results. 1, $E = 0.16$, $T = 873$ K; 2, $E = 0.2$, $T = 823$ K; 3, $E = 0.23$, $T = 748$ K.

range for the case of $q = 2.5$ and $\Delta Q = 26\,\text{kJ mol}^{-1}$. In contrast, if Gifkins [6] model is used to construct the $E = 0.5$ contours, there is marked disagreement with the experimental results; for this model E contours have slopes of $+b/m = 0.5$ when $d \neq a$ and for the case of $d = a$ the slope is zero.

The deformation mechanism map (Fig. 8) constructed using Langdon's [7] model predicts that a dynamic recrystallization can lead to a change of dominant deformation mechanism from dislocation creep to GBS in the temperature range 473 to 623 K. For example, at 473 K, $\sigma = 50$ MPa, Magnox Al80 with a starting grain size 100 μm, would recrystallize to $d \sim 10$ to 15 μm, a grain size within the dominant GBS field. In contrast, at higher temperatures, $T > 723$ K, the grain size developed by dynamic recrystallization is always within the dislocation creep field except possibly at very low stress, $\sigma < 0.9$ MPa, which is close to the stress at which diffusion creep mechanisms become dominant in this alloy [32].

4.4. Application to other materials

There is very little experimental information on the importance of GBS in other materials which undergo dynamic recrystallization. Some data are available for calcite [8, 22] which is often deformed by creep with concurrent recrystallization during geological processes. Schmid *et al.* [8] found that GBS accommodated between 12 and 54% of the imposed deformation in Carrara marble deformed at $T = 1273$ to 1073 K and $\sigma = 60$ to 5 MPa. A plot of the data for $\log(1/E - 1)$ against $\log \sigma$ (Fig. 9a) gives the value of $p - q = 1.43$ at 1273 K. In this regime $p = 4.2$ thus $q = 2.8$. The temperature dependence of E can be estimated from a plot of $\log_e(\psi\sigma^{-(p-q)})$ against $1/T$, where $\psi = (1/E - 1)$ (Fig. 9b). The value of ΔQ obtained depends strongly on the data point for 873 K where $E = 0$ was reported [8]. This corresponds to E less than the detectable limit, which could range from $E = 0.01$ to 0.001. The temperature dependence obtained ranges from $\Delta Q = 0$ to $133\,\text{kJ mol}^{-1}$ (Fig. 9b).

Deformation mechanism maps have been constructed for different values of the grain-size dependence of sliding (m). There are two stress recrystallized grain size relationships for calcite. One according to Schmid *et al.* [8] applies to a rotation recrystallization

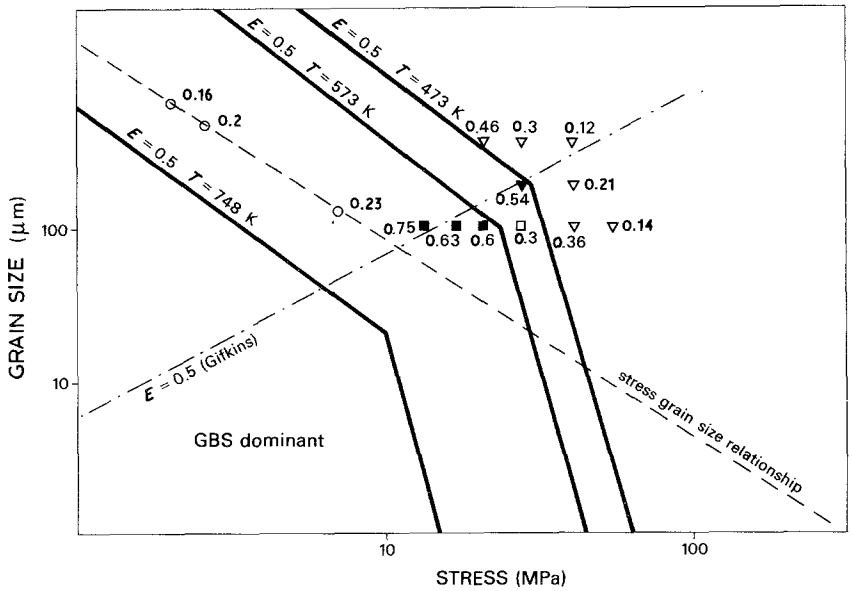

Figure 8 Deformation mechanism for Magnox Al80, with $E = 0.5$ contours constructed for $\Delta Q = 26\,\text{kJ mol}^{-1}$, $q = 2.6$ and temperatures of 748, 573 and 473 K. The positions of the contours are constrained by the experimental results of Bell and Langdon [4] at $T = 473$ to 573 K and from this study at $T > 740$ K. 473 K: (▽) $E < 0.5$, (▼) $E > 0.5$. 573 K; (□) $E < 0.5$, (■) $E > 0.5$. 748, 823, 873 K: (●) $E \sim 0.2$.

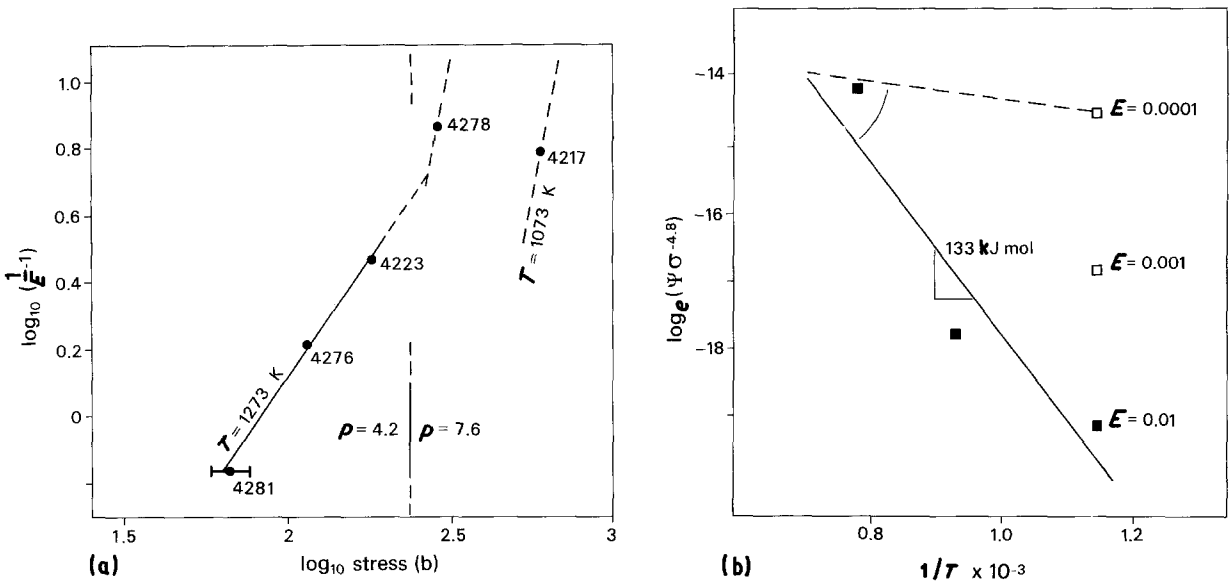

Figure 9 (a) A plot of $\log_{10}(1/E - 1)$ against $\log_{10}\sigma$ (in bars) for calcite [8]. According to Langdon's [7] model the experimental results for each temperature should lie on a straight line of slope $p - q$. Numbers next to the data points are the test identification from Schmid *et al.* [8]. (b) Temperature dependence of E in calcite from [8]. The data points should lie on a straight line of slope $-\Delta Q$. $q = 2.8$.

mechanism [33, 34], while the other [35] probably involves a type of migration recrystallization. Contours for $E = 0.5$ are drawn for $T = 1273$, 1113, 963 and 689 K for the two cases $m = 1$, $\Delta Q = 133\,\text{kJ mol}^{-1}$ (Fig. 10) and $m = 2.5$, $\Delta Q = 133\,\text{kJ mol}^{-1}$.

For the temperature independent case, the $E = 0.5$, $T = 1273$ K contour applies to all temperatures. The maps shown (Fig. 10) are drawn for the maximum temperature dependence consistent with the data of Schmid *et al.* [8].

The position of the GBS dominant field varies dramatically depending on the values of m and ΔQ used. In all cases the maps predict that GBS will be dominant in rotation recrystallized calcite when deformed at stresses < 25 MPa, i.e. when the recrystallized grain size is greater than 20 μm. This conclusion is opposite to the situation normally proposed where dominance of GBS is expected in fine-grained recrystallized materials. This effect arises because E is both stress and grain-size dependent [4, 22].

Extrapolation of the calcite deformation mechanism maps to geological conditions ($T \sim 473$ to 673 K), $\sigma =$ (1 to 200 MPa) would suggest that GBS accommodated by dislocation creep is an important process in many calcite-rich rocks. There may be problems, however, in extrapolation of the very high-temperature experimental results to lower temperatures. In particular, melt phases may be present at 1273 K in calcite [36]. If a melt phase were present along grain boundaries this may enhance the role of grain-boundary sliding, in comparison to a fluid-free aggregate. On the other hand, the operation of GBS is difficult to detect from microstructural information, so that naturally deformed calcite rocks, with well-developed dislocation creep microstructures, could also have deformed by significant GBS. In this respect certain microstructures such as diamond grain structures [37, 38] can be used as indicators of the operation of GBS.

5. Conclusions

1. During high-strain deformation of Magnox Al80 at elevated temperatures ($T > 0.6\,T_m$) dynamic recrystallization occurs with the resultant grain size related only to the flow stress. Under these conditions 16% to 23% of the imposed deformation is accommodated by grain-boundary sliding (GBS) with the remainder accommodated by dislocation creep. In a series of tests at constant strain rate, the importance of GBS increases as temperature decreases, stress increases and dynamically recrystallized grain size decreases.

2. The theoretical models developed by Gifkins [6] and Langdon [7], for the importance of GBS during creep can be simply modified to take account of the occurrence of dynamic recrystallization. In the modified form of Gifkin's [6] model the importance of GBS is dependent only on the flow stress, while in the modified form of Langdon's [7] model, the importance of GBS is dependent upon the flow stress and possibly temperature.

3. Comparisons between the modified theoretical models and the experimental results on Magnox Al80 show that the best fit to the available data on GBS can be obtained with Langdon's [7] model.

4. Deformation mechanism maps have been constructed for Magnox Al80 using the modified form of Langdon's [7] model calibrated by the experimental results. The maps predict that the occurrence of dynamic recrystallization can lead to a switch from dominant dislocation creep to dominant GBS at intermediate temperatures ($T =$ 673 to 473 K) and low stress. In contrast at higher temperatures the large grain size produced by dynamic recrystallization limits the importance of GBS.

5. Deformation mechanism maps have been constructed for calcite ($CaCO_3$) based on the modified form of Langdon's [7] model and the experimental results of Schmid *et al.* [8]. The maps predict that GBS should be the dominant deformation mechanism in

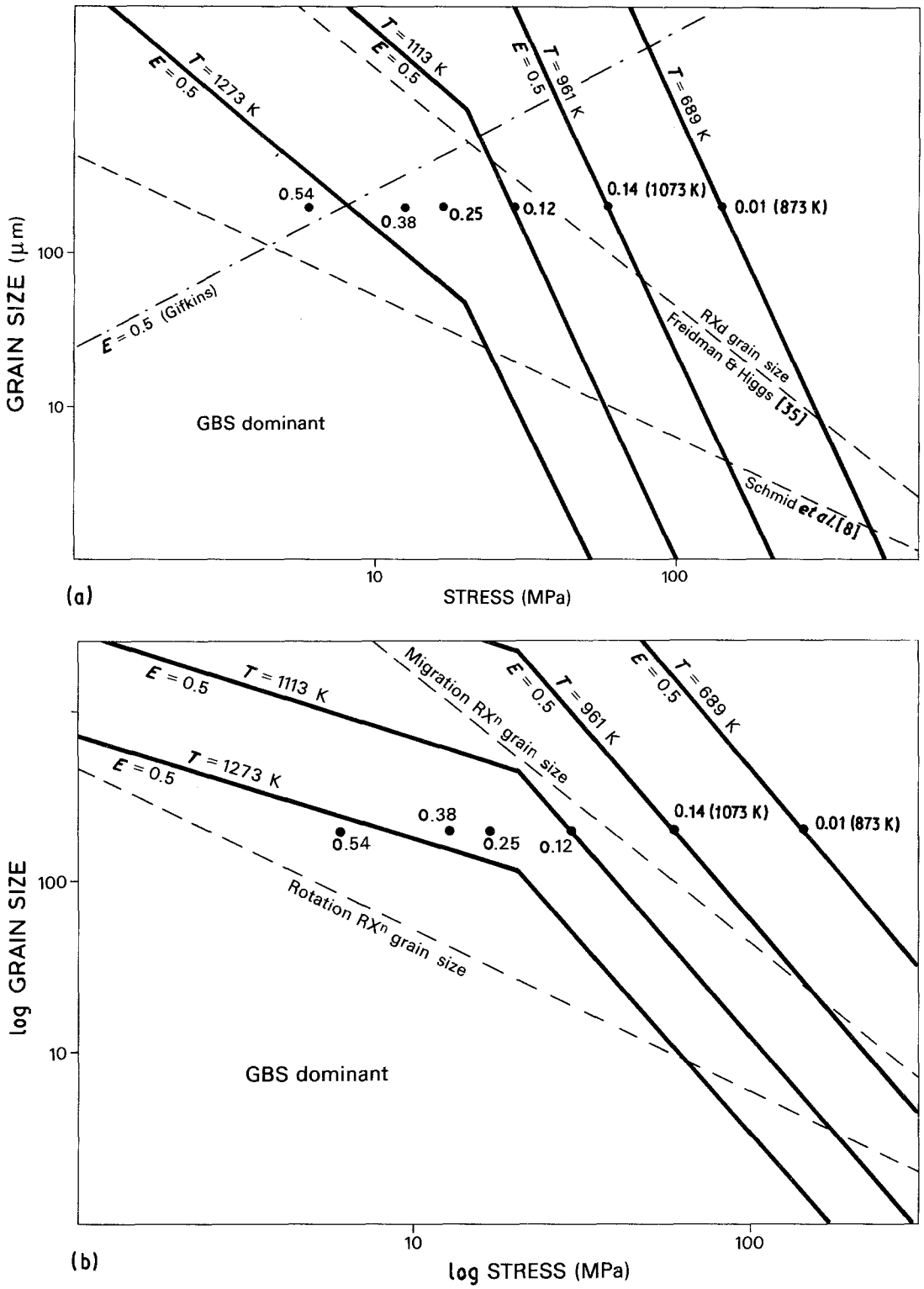

Figure 10 Deformation mechanism maps for calcite constructed using Langdon's [7] theory constrained by the results of Schmid *et al.* [8]. (a) For case $m = 1$, $\Delta Q = 133\,\text{kJ mol}^{-1}$. (b) For case $m = 2.5$, $\Delta Q = 133\,\text{kJ mol}^{-1}$.

naturally deformed calcite at stresses less than 25 MPa, when complete rotation recrystallization has occurred. The validity of this prediction depends on an extrapolation from $T = 1273$ K to geological conditions of 473 to 673 K. It is possible that the presence of grain-boundary melt phases in the high-temperature experiments invalidates this extrapolation.

Acknowledgements

The experimental work was conducted in the Department of Metallurgy and Material Science, Imperial College, London. An NERC (Natural Environment Research Council) Research Studentship (GT4/79/GS.64) held by M. R. D. during this period is gratefully acknowledged. Hans de Bresser is thanked for discussions and comments on the original manuscript.

References

1. D. McLEAN, *J. Inst. Metals* **80** (1951-52) 507.
2. B. FAZAN, O. D. SHERBY and J. E. DORN, *Trans. Amer. Inst. Min. Eng.* **200** (1954) 919.
3. H. BRUNNER and N. J. GRANT, *ibid.* **218** (1960) 122.
4. R. L. BELL and T. G. LANGDON, *J. Mater. Sci.* **2** (1967) 313.
5. R. N. STEVENS, *Metall. Rev.* **II** (1966) 129.
6. R. C. GIFKINS, *J. Aust. Inst. Metals* **17** (1973) 137.
7. T. G. LANGDON, in "Rate processes in plastic

formation of materials", The J. E. Dorn Symposium (ASM, 1975) p. 410.
8. S. W. SCHMID, M. S. PATERSON and J. N. BOLAND, *Tectonophys.* **65** (1980) 245.
9. P. W. DAVIES, R. N. STEVENS and B. WILSHIRE, *J. Inst. Metals* **94** (1966) 49.
10. R. C. GIFKINS, *J. Inst. Metals* **87** (1958-59) 255.
11. C. M. SELLARS, *Phil. Trans. R. Soc. Lond.* **288A** (1978) 147.
12. T. SAKAI and J. J. JONAS, *Acta Metall.* **32** (1984) 189.
13. R. J. TWISS, *Pure Appl. Geophys.* **115** (1977) 143.
14. S. H. WHITE, *Tectonophys.* **39** (1977) 143.
15. M. R. DRURY, F. J. HUMPHREYS and S. H. WHITE, *Phys. Earth Planet. Int.* **40** (1985) 208.
16. B. DERBY and M. F. ASHBY, *Scripta Metall.*, in press.
17. S. H. WHITE, *Phil. Trans. R. Soc. Lond.* **283A** (1976) 69.
18. M. HATHERLEY, A. S. MALIN, C. M. CARMICHAEL, F. J. HUMPHREYS and J. HIRSCH, *Acta Metall.* **34** (1986) 2247.
19. S. H. WHITE, S. E. BURROWS, J. CARRERAS, N. D. SHAW and F. J. HUMPHREYS, *J. Struct. Geol.* **2** (1980) 175.
20. J. P. POIRIER, *J. Struct. Geol.* **2** (1980) 135.
21. S. E. ION, F. J. HUMPHREYS and S. H. WHITE, *Acta Metall.* **30** (1982) 1909.
22. S. M. SCHMID, J. N. BOLAND and M. S. PATERSON, *Tectonophys.* **43** (1977) 257.
23. C. J. SPIERS, *Bull. Mineral.* **102** (1979) 282.
24. T. G. LANGDON, *Metals Forum* **4** (1981) 14.
25. R. L. BELL, C. GRAEME-BARBER and T. G. LANGDON, *Trans. Amer. Inst. Min. Eng.* **239** (1967) 1821.
26. T. G. LANGDON, *Metall. Trans.* **3** (1972) 797.
27. M. R. DRURY, PhD thesis, University of London (1984) unpublished.
28. C. GRAEME-BARBER, PhD thesis, University of London (1967) unpublished.
29. J. L. WALTER and H. E. CLINE, *Trans. Met. Soc. Amer. Inst. Min. Eng.* **242** (1968) 1823.
30. F. W. CROSSMAN and M. F. ASHBY, *Acta Metall.* **23** (1975) 425.
31. S. S. VARIGALI and T. G. LANGDON, *ibid.* **30** (1982) 1157.
32. J. E. HARRIS and R. B. JONES, Report no. RD/B/R, 144 (1963), CEGB Berkeley Nuclear Laboratories.
33. J. P. POIRIER and M. GUILLOPE, *Bull. Mineral.* **102** (1979) 67.
34. P. D. TUNGATT and F. J. HUMPHREYS, *Acta Metall.* **32** (1984) 1625.
35. M. FRIEDMAN and N. H. HIGGS, *EOS Trans. Amer. Geophys. Un.* **61** (1981) 375.
36. D. L. OLGAARD and B. EVANS, *J. Amer. Ceram. Soc.* **69** (1986) C-272.
37. V. SINGH, P. RAMA-RAO, G. J. COCKS and D. M. R. TAPLIN, *J. Mater. Sci.* **8** (1977) 373.
38. M. R. DRURY and F. J. HUMPHREYS, *J. Struct. Geol.* **10** (1988) 83.

Received 27 October 1987
and accepted 23 February 1988